scientific reports

Check for updates

OPEN

Study on the formation mechanisms and stability of a gently inclined and shallow accumulative landslide

Mengxiao Zhang[1], Weizao Wang[1,2,3]✉, Yinbo Hao[4], Xiaoyang Liu[1], Ruisong Zhang[1], Zhaomin Tian[1], Minuo Huang[1] & Jinmeng Zhang[1]

The extremely heavy rainstorm on September 16, 2011, in Nanjiang County, Sichuan Province, induced many accumulative landslides. Most of these slopes were 3 ~ 5 m thick, sliding along the soil–bedrock interface, and the dip angle of the sliding bed was 10 ~ 20°. To study the reasons for and stability of this type of landslide, which mainly involved sliding along the soil–bedrock interface, this paper took the Qiling Village landslide as an example and conducted shear tests on the sliding bodies, sliding zone soils, and bedrock interfaces with different moisture contents and numerically simulated the stability of the slope.The research results revealed that the shear strength of the sliding soil and the soil–bedrock interface decreased with increasing moisture content. The shear strength of the sliding soil–smooth bedrock interface was the smallest; therefore, the landslide slid along the sliding soil–smooth bedrock interface. Under the action of heavy rainfall, the water level continued to rise, and the pore water pressure gradually increased. The coupling of pore water pressure and rainwater softening caused the Qiling Village landslide. The stability of the slope was greatly affected by pore pressure in the early stage of rainfall, and the influence of rainwater softening was greater in the later stage.

Keywords Gently inclined shallow landslide, Soil-bedrock interface, Failure mechanism, Stability

As one of the main triggering factors for landslides, large-scale landslide disasters caused by rainfall have become increasingly common in recent years[1–4]. Landslides induced by rainfall are characterized by strong suddenness, group occurrence, and destructiveness[5,6]. Heavy rainfall has played a key controlling role in many catastrophic landslides in southwestern China in recent years[7–9]. There have been widespread occurrences of gently inclined and shallow accumulative landslides that have slid along the soil-bedrock interface in western China[10–15], resulting in serious casualties. For example, the 2011 Nanjiang "9.16" extremely heavy rainstorm triggered thousands of landslides in the gently shallow accumulation layer, causing 9 people to be missing[16–20]. Since the 1980s, there have been more than ten gently inclined and shallow accumulative landslides in the Sichuan Basin, resulting in more than a thousand casualties. Therefore, studying the formation mechanisms and stability of gently inclined and shallow accumulative landslides induced by heavy rainfall sliding along soil-bedrock interfaces is highly important.

Direct shear tests of the soil-structure interface are the main way to study the mechanical properties of the interface, and many scholars have conducted many studies on the mechanical properties of the soil-structure interface[21–26]. Shear tests at the soil-structure interface are mainly concentrated at the soil-concrete, soil-geotextile, and soil-steel interfaces[27–31]. These experimental results have deepened our understanding of interface shear characteristics[32,33]. However, traditional direct shear tests and interface shear tests conducted by previous researchers have relatively small shear displacements. The improved direct shear instrument in this study has a larger shear displacement, which can better simulate the process of shear between the sliding zone soil and the bedrock surface. In addition, there are few studies on the shear between the sliding zone soil-the bedrock interface in landslides, and in-situ testing of the shear between the sliding zone soil- the bedrock interface is

[1]School of Urban Geology and Engineering, Hebei GEO University, Shijiazhuang 050031, China. [2]Hebei Technology Innovation Center for Intelligent Development and Control of Underground Built Environment, Shijiazhuang 050031, China. [3]Key Laboratory of Intelligent Detection and Equipment for Underground Space of Beijing-Tianjin-Hebei Urban Agglomeration, Ministry of Natural Resources, Shijiazhuang 050031, China. [4]Hebei Geo-Environment Monitoring Institute, Shijiazhuang 050022, China. ✉email: wangvz2005@126.com

very difficult. Therefore, further research is still needed on the shear characteristics of the sliding zone soil and bedrock surface under large shear displacement.This paper considers sliding zone soils with different moisture contents and bedrock with different roughness. Through improved direct shear tests, the shear mechanical properties of the sliding zone soil–bedrock interface under different moisture contents were studied.

Numerical simulation technology has been widely used in the study of landslide disasters due to its convenient, fast, and accurate modeling and calculation characteristics.The commonly used numerical simulation software in landslide stability currently includes Flac3D, Slide, ABAQUS, Ansys, Geo-Studio, etc[34–36].The seepage analysis module (SEEP/W), stress deformation analysis module (SIGMA/W), and slope stability analysis module (SLOPE/W) included in Geo-Studio can be analyzed independently or called upon each other, and are widely used for analyzing slope stability[37,38].

The failure mechanism of shallow landslides is related to the strength shear of the landslide body and sliding zone soil, and recent research has mostly focused on the influencing factors of landslides, which cannot explain the specific failure characteristics of the Qiling village landslide.There are many research methods for the stability of shallow landslides, but recent studies have mostly used engineering analogy, limit equilibrium method, and numerical simulation method. Numerical simulation method mainly studies the stability of landslides from stress, deformation, displacement of slopes, but there is relatively little research on landslide stability based on unsaturated seepage theory.Although a series of investigations have been conducted on the formation factors and distribution patterns of the accumulation layer landslide that occurred in Nanjiang[17,18].The failure mechanisms and stability of gently inclined and shallow landslides sliding along the soil-bedrock interface still need further exploration.

The research methodology and proposed research results in this paper are highly innovative.In this article, we attempt to reveal the sliding instability mechanism of this type of landslide along the soil-bedrock interface from the perspective of strength based on the characteristics of landslide failure in gentle and shallow accumulation layers. Therefore, this study conducted a series of shear tests on sliding soil, sliding zone soil, and sliding zone soil- bedrock interface using a multifunctional testing device and an improved direct shear device. In addition, there is relatively little research on the shear between landslide sliding zone soil and bedrock interface, and this study enriches the research in this area.We conducted a study on landslide stability based on unsaturated seepage theory in order to study the influence of rainfall on the stability of gentle shallow accumulation slopes. This paper analyzed the changes in pore water pressure at the soil-bedrock interface and the dynamic changes in soil infiltration lines of the Qiling Village landslide, and calculated the transient stability of the slope by combining the SEEP/W and SLOPE/W modules of Geo-Studio finite element software.These research results are important for the formation mechanism and stability analysis of soil slopes sliding along the soil-bedrock interface, and will provide technical references for future research.

Study area

Geological setting

The Qiling village landslide is located in Nanjiang County, Sichuan Province, China (Fig. 1).

The landform in the landslide area consists of shallow-to-medium cut and eroded moderate-to-low mountains, with slow-inclination single-sided mountains, with elevations ranging from 1060 to 1320 m. The bedrock is mainly composed of interbedded sandstone and mudstone, with relatively flat rock layers ranging from 10° to 20°, with a slope angle smaller than the longitudinal slope angle. The surrounding areas of the mountain are mostly in a stepped shape. The exposed strata in the landslide area include the Quaternary residual slope loose accumulation layer (Q_4^{dl+cl}) and the Cangxi Formation of the Early Cretaceous age (K_1C). The Quaternary residual slope loose accumulation layer (Q_4^{dl+cl}) is composed mainly of silty clay interbedded with fragmented stones.The lithology of the Cangxi Formation (K_1C) of the Early Cretaceous age is interbedded with sandstone and mudstone, with a thickness of 10–40 m and the rock attitude of 320 ° -360 °∠ 10 ° -15 °.

Hydrological conditions

The landslide area has abundant precipitation, with an annual rainfall of 1198.7 mm. Precipitation is concentrated from May to October. The main types of groundwater are bedrock fissure water and loose soil layer pore water. Quaternary pore water mainly exists in soil layers, receives atmospheric precipitation recharge, and flows from high-elevation areas to low-elevation areas. Bedrock fissure water mainly exists in weathered fissures and unloading fissures of bedrock, is supplied by atmospheric precipitation and overlying Quaternary pore water, and is discharged along slopes.

Characteristics of the gently inclined shallow accumulative landslides

Boundary and scale of the landslide

The rear edge of the landslide is a steep slope with a gradient of approximately 35°. There are many solitary stones on the slope, and the vegetation is relatively developed. The rear edge of the landslide is bounded by a steep wall (Fig. 2), and the landslide body forms a "tongue" shape on the plane (Figs. 3 and 4). The landslide was divided into upper and lower parts, with the upper sliding bed exposed and the middle and lower parts being accumulation bodies. The boundaries of the landslide were obvious. The elevation of the landslide rear edge is 1220 m, and the elevation of the front edge shear outlet is between 1080 and 1100 m, with a difference of 130 m in elevation between the front and rear edges. The upper part of the landslide is relatively gentle, ranging from 13° to 16°, with the local maximum reaching 25°. The lower part is slightly steeper, ranging from 19° to 24°. The front edge of the landslide is a rice field and a small gully, forming the free face of the landslide. The upper part of the landslide is 146 m long and 55 m wide, and the lower part is 248 m long and 64 m wide, with an area of approximately 24,000 m^2. The main sliding direction of the landslide is 0°, and the thickness is approximately 1–5 m. The estimated volume of the landslide is approximately 7.2×10^4 m^3, which represents a small landslide.

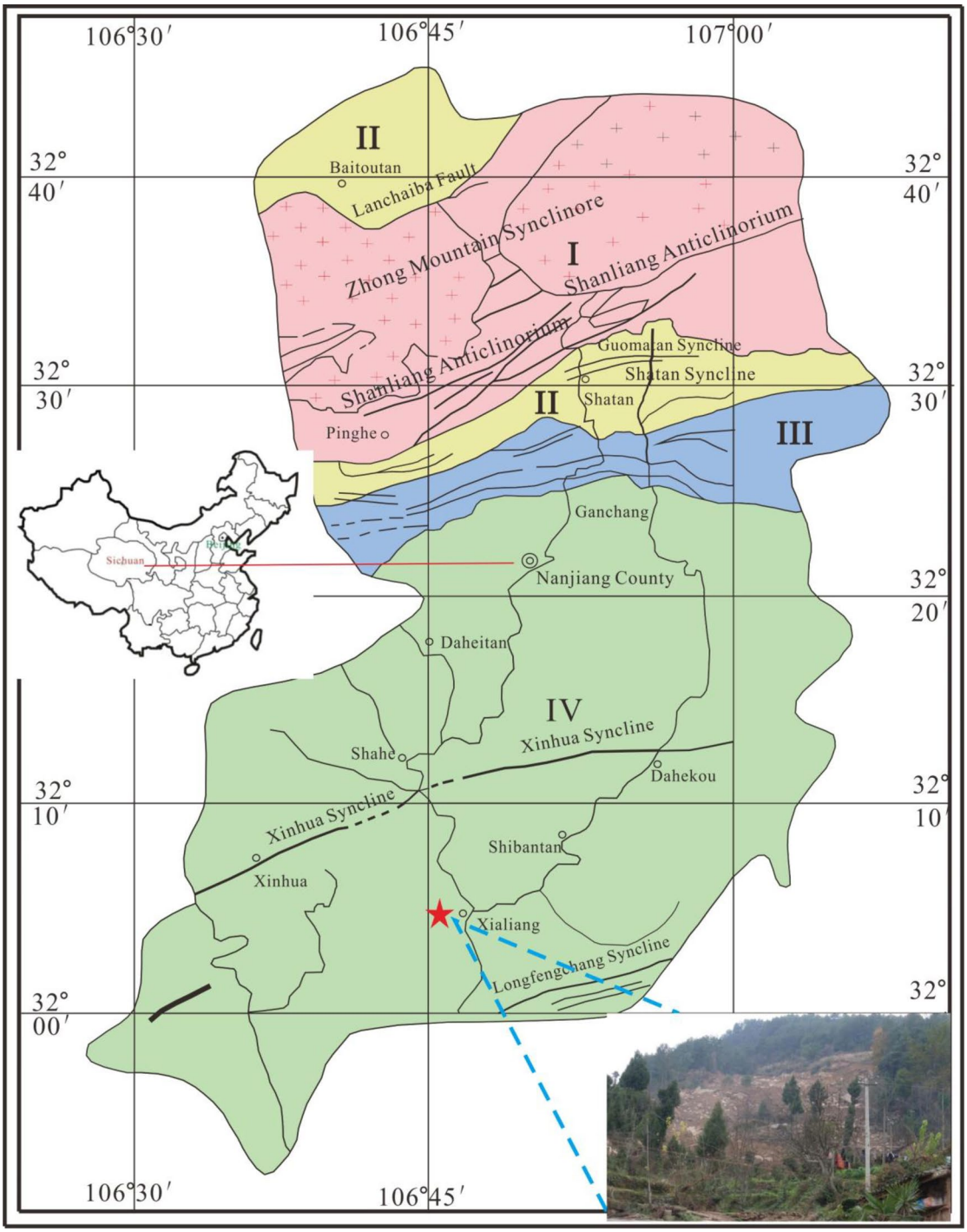

Fig. 1. The geological map of the landslide area.

Characteristics of the slip zone

The sliding zone was located at the silty clay–bedrock interface according to field investigations. The slip zone soil is a mixture of powdery clay and a small amount of gravel. The soil texture of the local sliding soil is uneven, with rough cut surfaces and traces of rubbing; the soil feels smooth and wet and is in a soft plastic flow state. The middle part of the sliding surface (belt) has a deep burial depth, whereas the front and rear parts are relatively small. The longitudinal section has a folded line shape (Fig. 5) with slight undulations.

Characteristics of the sliding beds

The landslide bed was located in the Cangxi Formation of Cretaceous age (K_1C), which is composed of brownish red and purple red mudstone, silty mudstone, thick blocky medium- to fine-grained feldspar quartz sandstone, lithic sandstone, and conglomerate according to field investigations. The upper sliding bed of the landslide was exposed (Fig. 6a), which was composed of gray white and gray yellow medium- to fine-grained

Fig. 2. The rear edge of the landslide.

Fig. 3. Overview of Qiling Village landslide.

feldspar quartz sandstone, lithic sandstone, and conglomerate with obvious scratches. The attitude of the sliding bed is 320°∠ 15°. The lower part of the landslide has almost no exposed sliding bed, with occasional exposure in some areas (Fig. 6b). The exposed sliding bed is composed of purple red mudstone, siltstone, and siltstone, with an attitude of 357°∠ 24°.

Deformation characteristics of the landslide

The Qiling village landslide was divided into source zones, sliding zones, collapse zones, and deposition zones according to the deformation characteristics of the landslide (Fig. 4).

The source zones were located at the rear of the landslide, with a transverse width of approximately 55 m, a longitudinal length of 82 m, and a plane area of 4510 m^2. The thickness of the landslide body was small, ranging from 0.5 to 1 m. It was thick at the top and thin at the bottom in the vertical direction and thick on both sides and thin in the middle in the horizontal direction (Fig. 7). The main sliding direction of the landslide was 0°, with an overall slope of 15°, as shown in Fig. 8.

The sliding body in the sliding source zones formed accumulations of varying sizes, with obvious traces of soil movement and localized exposure of the sliding bed. The sliding body is mainly composed of loose deposits of Quaternary collapse and slope deposits, which consist of block gravel soil filled with angular gravel soil and sandy soil and are purple-red to yellow-brown in color (Fig. 8). The content of block stones ranges from 30 to 40%, with particle sizes ranging from 20 cm to 300 cm. The content of crushed stones ranges from 10 to 20%, with particle sizes ranging from 2 to 20 cm. The sorting and rounding are poor, and the contents of angular gravel, sandy soil, and silty clay soil range from 40 to 60%. The rock properties of block stones are mainly purple gray, light gray, grayish white fine sandstone and light gray, grayish white medium- to fine-grained feldspar quartz sandstone. Occasionally, purple-red silty mudstone is observed, which is consistent with the surrounding exposed bedrock lithology.

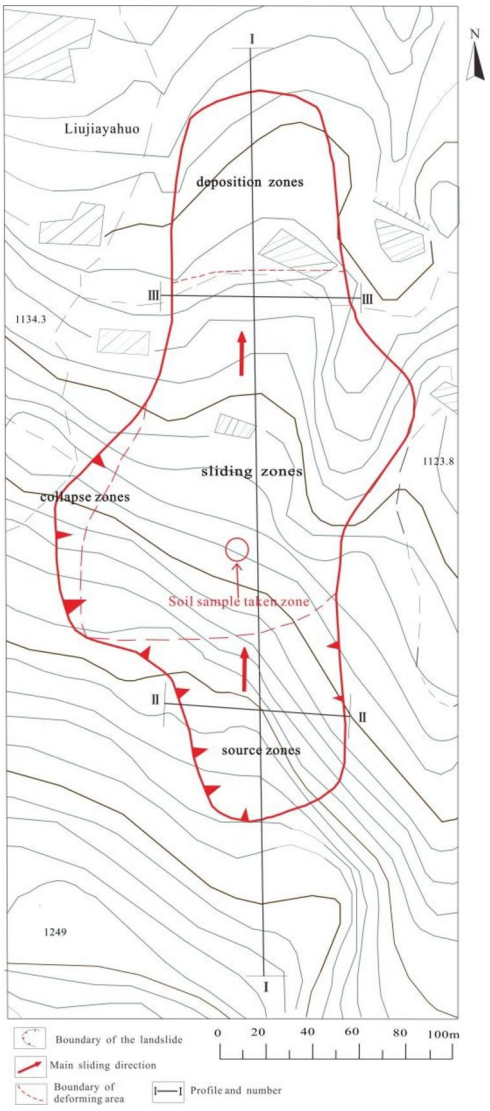

Fig. 4. Boundary of the Qiling village landslide.

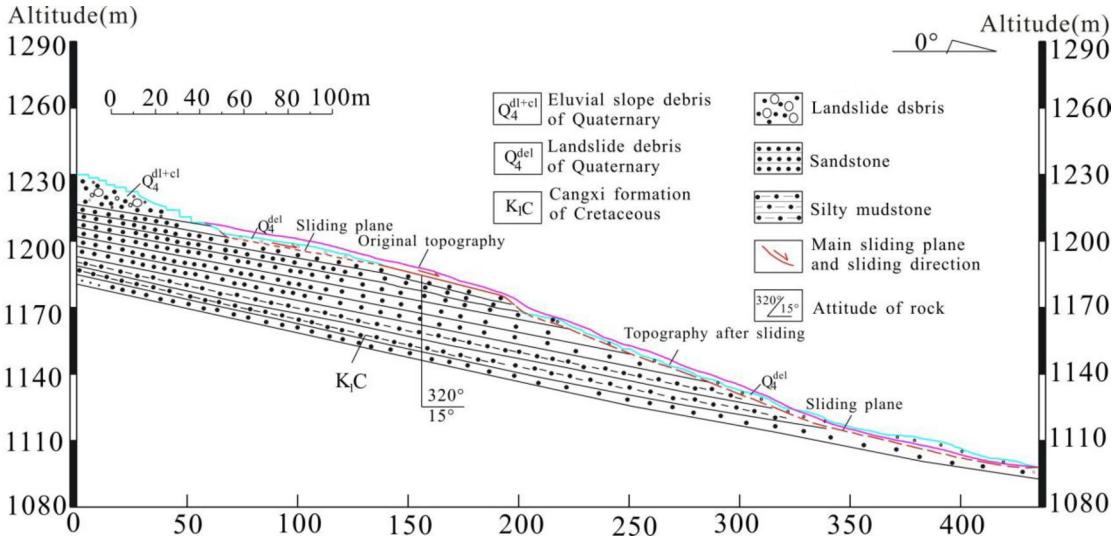

Fig. 5. I-I profile of the Qiling village landslide.

Fig. 6. Beds revealed on the back margin of the Qiling village landslide. (**a**) Exposed sliding bed of the upper landslide; (**b**) exposed sliding bed at the bottom of the landslide.

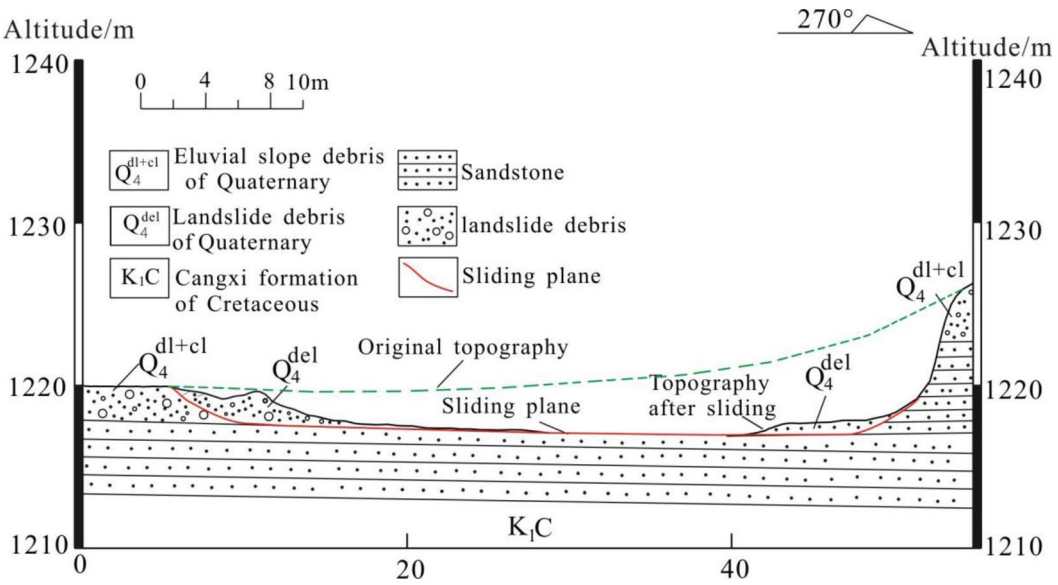

Fig. 7. II-II profile of the Qiling village landslide.

Fig. 8. Sliding source zones.

The sliding zone has a longitudinal length of 160 m and a width of approximately 64 m (Fig. 9). The total thickness of the landslide body is relatively small, with an average thickness of approximately 50 cm, and locally exceeds 1 m. It is thin in the longitudinal direction and thick in the lower part, with almost the same thickness in the transverse direction (Fig. 10). The traces of soil movement are obvious, and the local sliding

Fig. 9. Sliding zone.

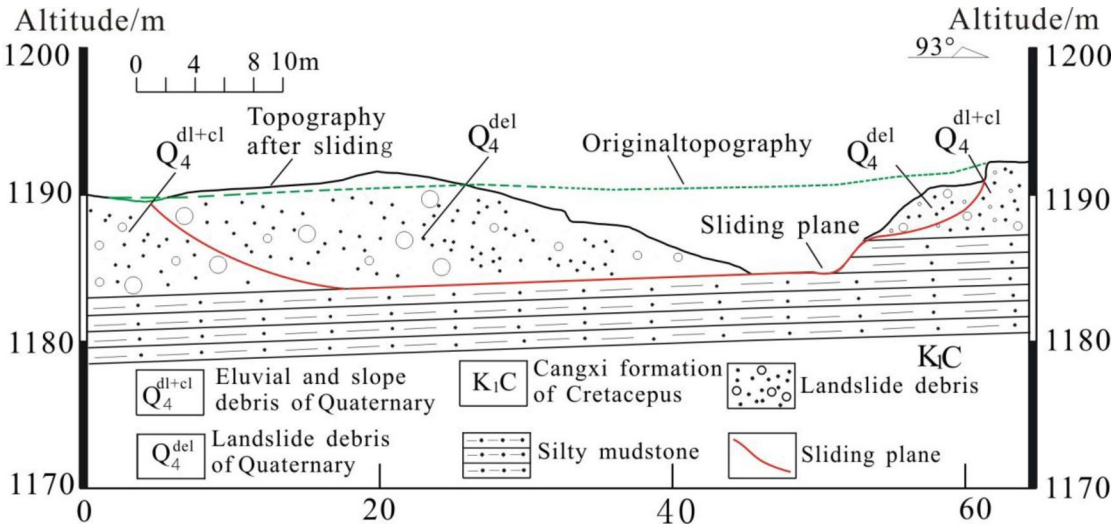

Fig. 10. III-III profile of the Qiling village landslide.

bed is exposed. The sliding body is mainly composed of loose accumulations of Quaternary collapse deposits and slope deposits, which consist of block gravelly soil filled with angular gravel soil and sandy soil and are purple-red to yellow-brown in color. The content of block stones ranges from 50 to 60%, with particle sizes ranging from 20 cm to 11 m. The content of crushed stones ranges from 10 to 15%, with particle sizes ranging from 2 to 20 cm. The sorting and rounding are poor, and the contents of angular gravel, sandy soil, and silty clay soil range from 25 to 40%. The rock properties of block stones are mainly purple gray, light gray, grayish white fine sandstone and light gray, grayish white medium- to fine-grained feldspar quartz sandstone. Occasionally, purple-red silty mudstone can be observed. The block stones have the same lithology as the bedrock at the rear edge and the sliding bed of the upper landslide. Many trees and woods are arranged horizontally and vertically in the sliding body. Water flows out of the sliding body, and the sound of water flow can be heard. The flow rate is approximately 0.5 L per second.

The deposition zones were located at the front of the landslide at the shear outlet of the front edge of the landslide (Fig. 11). The area was 79 m long and 62 m wide, with a thickness of 3–6 m and a volume of approximately 2.45×10^4 m^3. The accumulated material was gravelly soil, with gravel diameters ranging from 5 to 200 cm, including block stones with a maximum diameter of approximately 2 m. Many trees and small branches accumulated in the landslide area, and water flowed out of the landslide area at a flow rate of approximately 0.5 L per second.

The collapse zones were located on the upper left side of the landslide (Fig. 12), with a longitudinal length of 70–80 m. The accumulated material in the collapse area was powdery clay containing fragmented stones, with a maximum particle size of 40–50 cm. The content of fragmented stones was relatively high, reaching more than 50%. This area formed from traction after the main sliding body slid.

Fig. 11. Deposition zone.

Fig. 12. Collapse zone.

Materials and methods

Shear test

Experimental instruments

This shear tests included shear test of the sliding body and shear test at the soil-bedrock interface.The slope body of the Qiling village landslide is composed of crushed stone soil. Shear tests of the sliding body were conducted to obtain the shear strength parameters of the crushed stone soil. This experiment used a multifunctional tester (YDS-2) (shown in Fig. 13). This instrument can be used for gravel soil shearing with a particle size of less than 2.5 cm (as shown in Fig. 14). The moisture contents used in the experiments were 10%, 20%, 25%, and 30%.

An improved direct shear apparatus was used to shear two different surface roughness levels of the soil-bedrock interface in this experiment.The experiment used an improved strain-controlled direct shear apparatus (Fig. 15). The processed bedrock was placed in the lower box of the direct shear apparatus (Figs. 16, 17), and the soil was placed in the upper box. This could increase the shear area between the soil and the bedrock surface, reducing the error caused by the small shear area in the direct shear test. The bedrock was obtained from the sliding bed of the Qiling village landslide, and the bedrock was processed into 10 cm × 10 cm × 1 cm rock blocks. The rock samples used were divided into two types: rough bedrock and smooth bedrock (Fig. 16). The sliding soil was obtained from the boreholes of the Qiling village landslide. The moisture contents of the sliding soils used in the experiments were 10%, 20%, 25%, and 30%.

Preparation of samples

The sliding mass soil samples applied in this test were taken from the Qiling village landslide (Fig. 4). The physical parameters of the sliding mass soil samples are shown in Table 1. The particle size distribution curve of the sliding mass soil samples is shown in Fig. 18. The sliding mass soil was dried and sieved. Gravel larger than 2.5 cm was removed. The sliding mass soil was prepared with moisture contents of 10%, 20%, 25%, and 30%. The sliding mass soil was allowed to sit for 2 days with plastic wrap to allow the crushed stone soil to fully absorb moisture and ensure the uniformity of mixing between the soil and water after the sliding soil was prepared. The shear box was 15.7 cm long, 15.7 cm wide, and 15.3 cm high. The crushed stone soil was loaded into three layers and compacted layer by layer. The dry density of the soil samples was 1.83 g/cm^3.

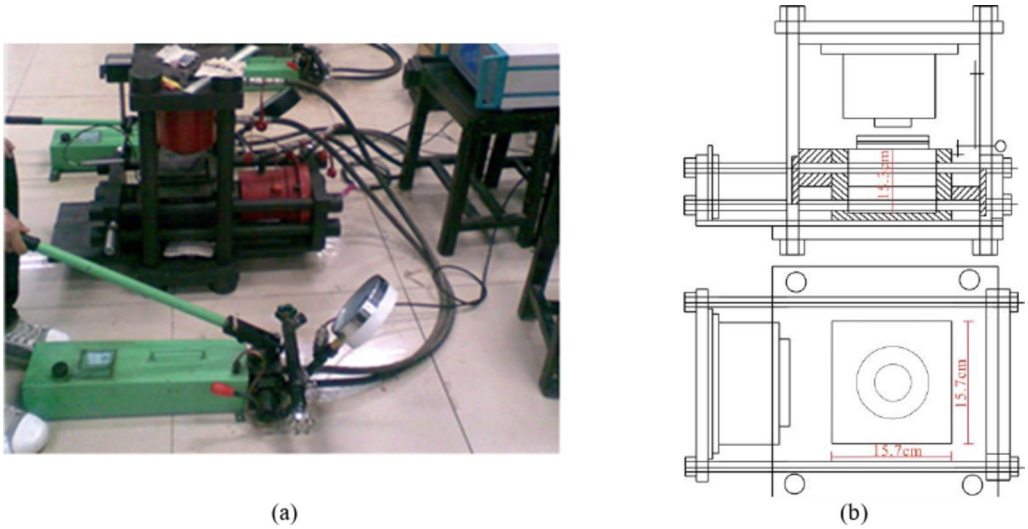

Fig. 13. Multi-functional tester. (**a**) Photos of testing equipment; (**b**) schematic diagram of the testing equipment.

Fig. 14. Sliding soil.

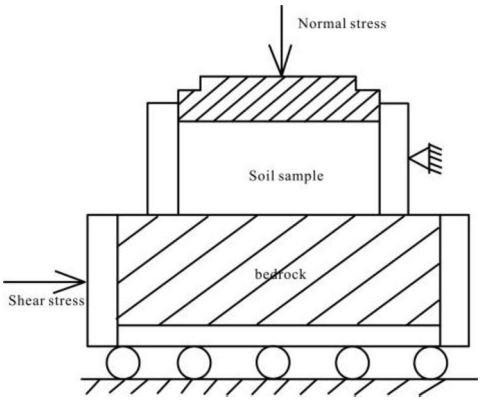

Fig. 15. Schematic diagram of improved direct shear apparatus for the soil–bedrock interface.

Fig. 16. Bedrock for the shear test. (**a**) Rough bedrock; (**b**) smooth bedrock.

Fig. 17. Bedrock in the lower box.

material name	natural density/g/cm^3	dry density g/cm^3	natural water content	permeability coefficient/cm/s
sliding body	2.16	1.775	20.4	3.66×10^{-5}
slippery soil	2.017	1.55	25.2	

Table 1. The physical parameter values for the slippery soil and sliding body.

The sliding zone soil samples applied in this test were taken from the Qiling village landslide (Fig. 4). The physical parameters of the sliding zone soil samples are shown in Table 1. The particle size distribution curve of the sliding zone soil samples is shown in Fig. 18. The sliding zone soil was dried and sieved. Gravel larger than 5 mm was removed. The sliding zone soil was prepared with moisture contents of 10%, 20%, 25%, and 30%. The sliding zone soil was allowed to sit for 2 days with plastic wrap to allow the crushed stone soil to fully absorb moisture and ensure the uniformity of mixing between the soil and water after the sliding soil was prepared. Circular soil samples with a diameter of 61.8 mm and a height of 20 mm were produced. The dry density of the soil samples was 1.83 g/cm^3.

Determination of the normal stress and shear stress

Each group of experiments consisted of five samples subjected to normal stresses of 100 kPa, 200 kPa, 300 kPa, 400 kPa, and 500 kPa in the shear test of the sliding body. The experiments could end upon reading 5–6 data after the peak value if the peak value was reached during the shearing process. The experiments could end with a shear displacement of 15 mm if there was no peak value during the shearing test.

The shear rate was 6 revolutions per minute, and the normal stresses were 100 kPa, 200 kPa, 300 kPa, and 400 kPa in the shear test at the soil-bedrock interface. The shear displacement had to be increased as much as possible during the test to better measure the shear strength between the sliding zone soil and the bedrock surface. The peak strength was the shear strength if there was a peak value. The shear stress corresponding to the maximum shear displacement was the shear strength if there was no peak value.

Analysis of experimental results

There were obvious shear bands in the sheared soil sample after the sample was sheared (as shown in Fig. 19). Their shear strengths are shown in Table 2. The shear strength index c of the sliding body first increased and

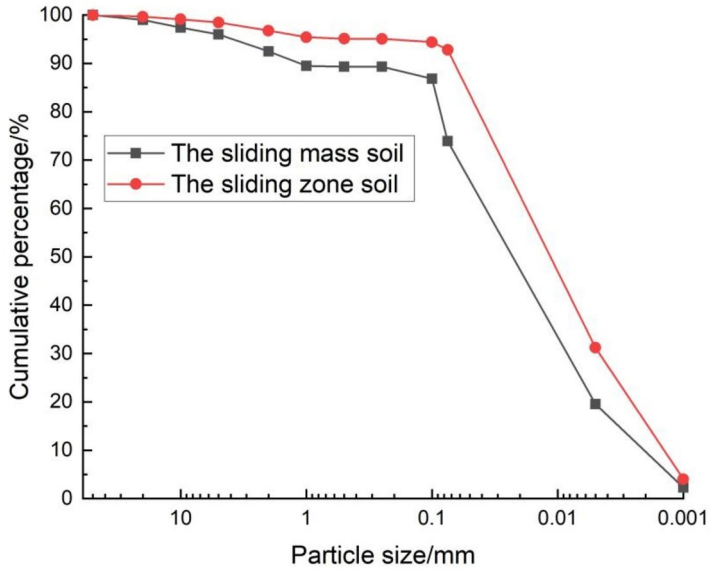

Fig. 18. Particle size distribution analysis.

Fig. 19. Soil sample after shearing.

Shearing type	Strength index	Moisture content/%			
		10%	20%	25%	30%
Sliding shear	φ/(°)	34.8	29.8	27.1	20.8
	c/kpa	45.8	46.5	43.0	35.9

Table 2. Shear strengths of the sliding bodies.

then decreased with increasing water content, whereas the value of φ decreased with increasing water content, according to Table 2.

The shear displacement and stress curves of each moisture content sliding zone soil and contact surface are shown in Figs. 20, 21, 22 and 23. The shear strength indicators c and φ of the sliding zone soil and each contact interface are shown in Table 3. The cohesive forces c of the sliding zone soil shear, sliding zone soil and smooth bedrock surface shear, and sliding zone soil and rough bedrock surface shear all increased first and then decreased with increasing water content, the φ decreased with increasing water content and the shear strength decreased with increasing water content according to Table 3. The variation patterns of the shear strength indicators c and φ at each contact interface were not good. For the convenience of comparing the shear strength of various contact interfaces, combined with the specific situation of the Qiling village landslide, a slope thickness of 5 m and a natural density of 2.0 g/cm^3 were taken as an example, which was equivalent to a normal stress of 100 kPa. The shear strength index was substituted into the shear strength formula to calculate the shear strength of each contact interface (Table 3).

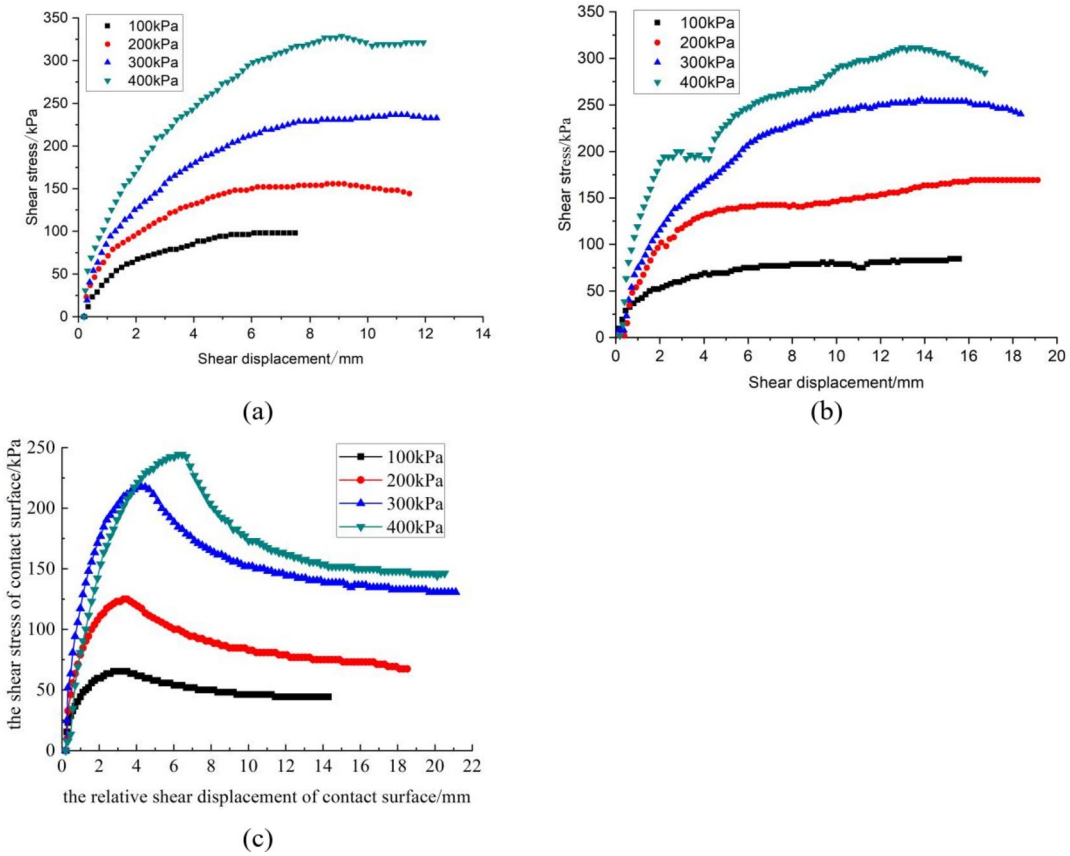

Fig. 20. Shear curve with a moisture content of 10%. (**a**) Slippery soil shear; (**b**) sliding soil–rough bedrock interface; and (c) sliding soil–smooth rough bedrock interface.

SS, SRB, and SSB represent the interfacial shear faces of the soil-to-soil, soil-to-rough bedrock, and soil-to-smooth bedrock samples, respectively. The shear strengths of the three contact interfaces were as follows: SRB > SS > SSB according to Table 3. This also indicated that the slope of the accumulation layer in the red layer area will slide along the boundary between the foundation and the cover when the bedrock surface of the sliding bed is smooth.

Stability analysis

Calculation methods and parameters

Because the thicknesses of the covering layer of this type of landslide were mostly 3–5 m, the longitudinal length of the landslide varied from tens to hundreds of meters, but these landslides slid along smooth base cover interfaces, and the inclination angle of the bedrock was 10–20°. This model was 150 m long and had a cover layer thickness of 5 m. The model involved two types of materials: the light green part in Fig. 24 is the gravel soil layer (cover layer), and the yellow part is the bedrock. The seepage analysis calculation adopted the finite-element method and adaptive meshing. The calculation model diagram is shown in Fig. 24.

The constitutive model for rock and soil used in the numerical simulation was the Mohr–Coulomb model. The bedrock was designated as a nonsliding layer. Two-dimensional stability analysis based on transient seepage analysis was conducted to simulate the instability processes of this landslide. The values of the model material parameters are shown in Table 4.The material parameters in Table 4 were obtained through a series of physical and mechanical experiments conducted on soil samples taken from the Qiling Village landslide in the laboratory .

In the seepage analysis, the moisture content of unsaturated soil was considered to have a significant effect on the soil properties, which further affects the possibility of landslides. Therefore, this study adopted unsaturated permeability analysis, assuming that the transient water flow in unsaturated soil during rainfall infiltration conforms to Darcy's law. In unsaturated flow, the permeability coefficient is a function of the water content or matric suction in unsaturated soil, whereas in saturated soil, it is usually assumed to be constant. For the soil–water characteristic curve, the Fredlund–Xing model was used. Figure 25a shows the soil-water characteristic curve and permeability curve from the seepage analysis. The boundary conditions of the two models are based on the actual rainfall data presented in Fig. 25b.

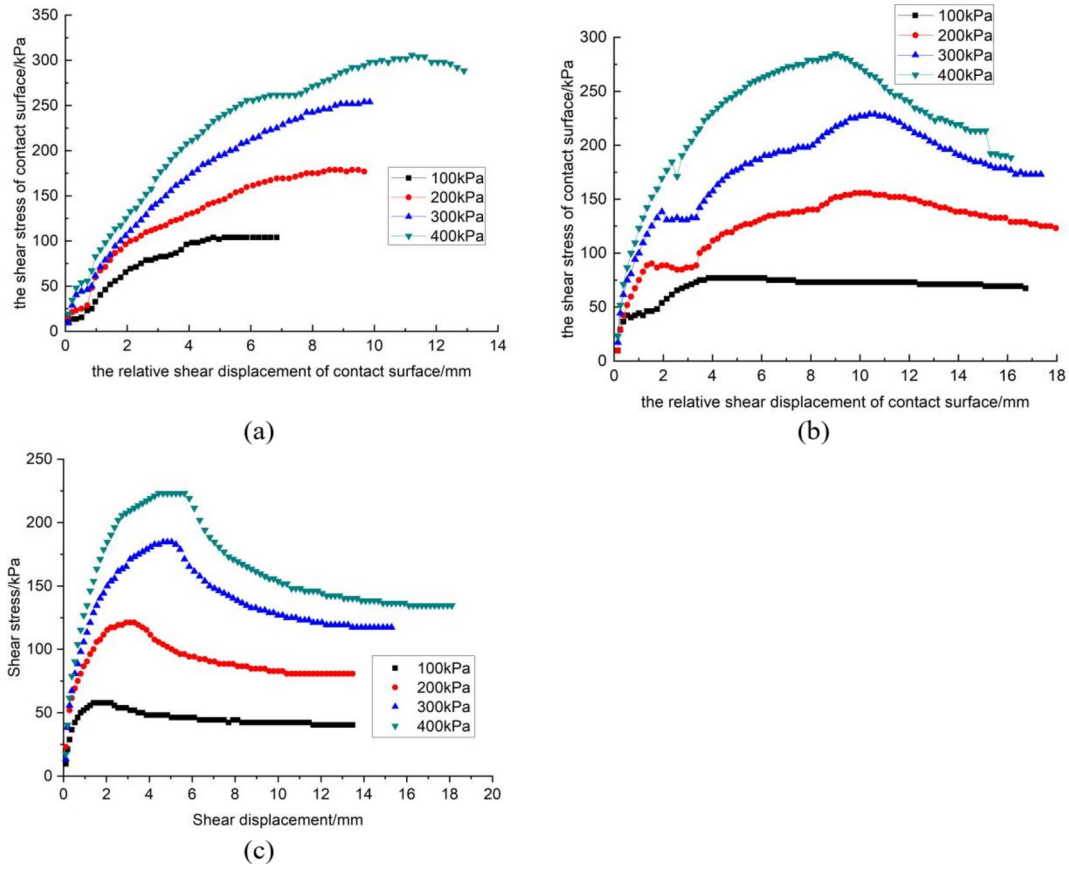

Fig. 21. Shear curve with a moisture content of 20%. (**a**) Slippery soil shear; (**b**) sliding soil–rough bedrock interface; and (c) sliding soil–smooth rough bedrock interface.

Simulation conditions of the seepage field

The Qiling village landslide occurred on September 18, 2011, and the rainfall conditions at the time of the landslide are shown in Fig. 26. Figure 26 shows the distribution of daily rainfall in Qiling village from July to September 2011. According to Fig. 26, the daily rainfall in Qiling village on September 17, 2011, was 250.4 mm, and the rainfall lasted for approximately 2 days. On the basis of the rainfall situation at the time of the Qiling village landslide, a rainfall intensity of 250 mm/d was selected for the model experiments, with 2 days of rainfall followed by 2 days of cessation of rainfall, for a total of 4 days of rainfall simulation.

Analysis of the simulation results of the seepage field

Variation law of the water head

The variation law of the water head is shown in Fig. 27. During heavy rainfall, rainwater flows from top to bottom. First, the soil is saturated at the soil-bedrock interface at the front edge of the slope, forming a transient saturated seepage field. As the rainfall continues, the saturated area continuously moves from the front edge of the slope along the soil-bedrock interface toward the middle and rear parts of the slope, and the water level continues to rise, gradually increasing the water head.The numerical simulation results are consistent with the on-site pore water pressure monitoring results.

Distribution law of the transient water level

The distribution law of the transient water level is shown in Fig. 28. Rainwater can quickly infiltrate the base cover interface through advantageous infiltration channels, and the permeability of bedrock is very low, playing a role in water isolation. Therefore, stagnant water is generated at the base cover interface, forming a transient water level. First, the front edge of the slope is saturated at the base cover interface, and as the rainfall continues, the saturated area continues to expand toward the middle and rear parts of the slope, and the water level line also continuously rises toward the surface.The numerical simulation results are basically consistent with the on-site investigation results of the landslide.

Two-dimensional stability analysis method

The simulation results of the seepage field were coupled with Slope/w, and then Slope/w was used to calculate its stability. The calculation blocks are shown in Fig. 29.

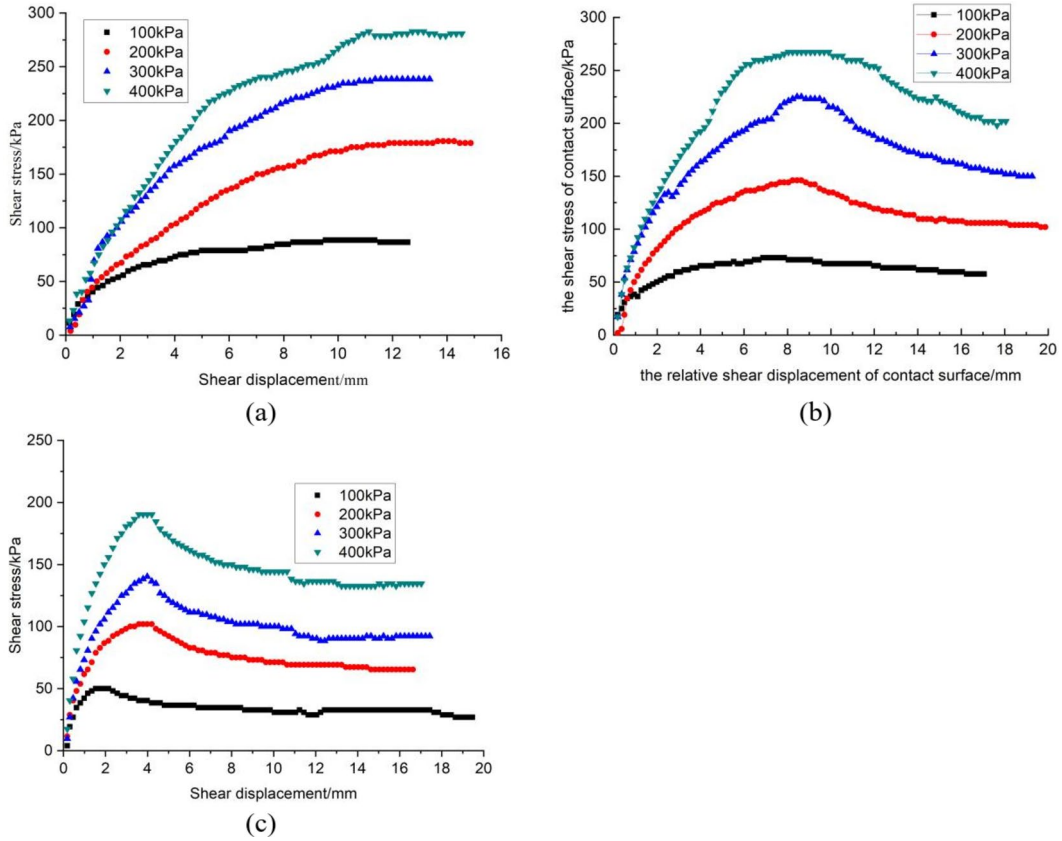

Fig. 22. Shear curve with a moisture content of 25%. (**a**) Slippery soil shear; (**b**) sliding soil–rough bedrock interface; and (**c**) sliding soil–smooth rough bedrock interface.

Result analysis

The stability coefficient of the 5-m accumulative slope with an increasing rainfall duration is shown in Fig. 30. The safety coefficient of the shallow accumulative slope was 1.816 before the heavy rainfall on September 16th, and it was in a stable state. As heavy rainfall began, rainwater quickly infiltrated through the dominant infiltration channel, increasing the moisture content of the slope soil. After 4 h of rainfall, the rainwater reached the soil-bedrock interface at the front edge of the slope, saturating the soil and increasing the pore water pressure. The stability coefficient of the slope slightly decreased; as heavy rainfall continued, rainwater gradually accumulated at the soil-bedrock interface of the slope. After the rainwater reached the soil-bedrock interface, the sliding soil gradually saturated and softened the sliding soil, resulting in a significant decrease in the shear strength index between the sliding soil and the bedrock surface. The loss of soil matrix suction and increase in pore water pressure at the soil-bedrock interface led to a decrease in the slope stability coefficient. When the rainfall lasted for 40 h, the stability coefficient of the soil slope decreased to 1.121, and at 44 h, the stability coefficient was 0.91, causing overall sliding of the slope. After the rain stopped, the accumulated water in the slope gradually seeped out, causing the groundwater level in the slope to gradually decrease, the pore water pressure to slowly decrease, and the stability coefficient of the slope to increase.The numerical simulation of landslide evolution stability process is consistent with the actual landslide instability process.

Discussion

The slope angle has a significant impact on the stability of the slope. In general, the stability of the slope decreases as the slope angle increases, and the stability of the slope improves as the slope angle decreases[7–9].However, a large number of accumulated landslides in Nanjiang County mainly occur at slope angles of 10°-20° under the influence of heavy rainfall[16–20], indicating that the formation mechanism of such landslides is very special.

The shear strength of soil decreases with the increase of moisture content. The physical mechanisms are as follows: the water forms a lubricant on the surface of the soil particles, reducing the frictional force between the soil particles, resulting in a decrease in the internal friction angle and thus reducing the shear strength of the soil when the moisture content increases; the bound water film adsorbed on the surface of soil particles will thicken due to the increase in water content, which weakens the intermolecular electric molecular force and leads to a decrease in cohesion, thereby reducing the shear strength of the soil; pore water pressure in the soil will increase due to the increase in water content, which may result in a decrease in effective stress and subsequently lower the shear strength of the soil from formula (1).

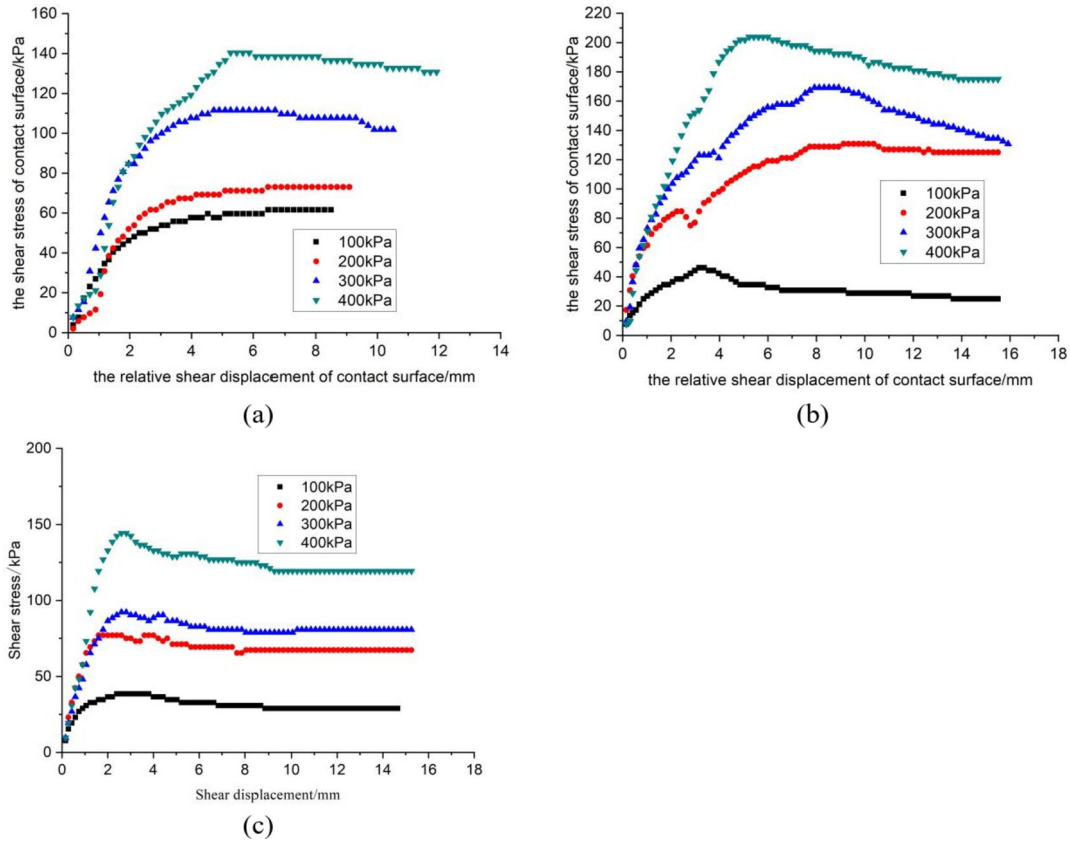

Fig. 23. Shear curve with a moisture content of 30%. (**a**) Slippery soil shear; (**b**) sliding soil–rough bedrock interface; and (**c**) sliding soil–smooth rough bedrock interface.

Interfacial shear	strength index	Moisture content/%			
		10%	20%	25%	30%
SS	$\varphi/(^\circ)$	28	22.9	20.7	15.7
	c/kpa	30.78	37.50	34.61	25.11
	τ/kpa	83.84	79.804	72.31	53.2
SRB	φ/(°)	37.5	34.6	33.5	27.1
	c/kpa	13.46	14.5	12.5	9.615
	τ/kpa	90	82.11	78.65	60.767
SSB	$\varphi/(^\circ)$	32.2°	29.23	24.68	18.4
	c/kpa	5.77	6.73	5.69	4.81
	τ/kpa	68.65	62.689	54.04	38.078

Table 3. Shear strengths of various contact interfaces.

$$\tau_f = \sigma' \tan\phi' + c' = ?\sigma - u?\tan\phi' + c' \quad (1)$$

Where τ_f is shear strength (kPa), σ' is the normal effective stress on the shear failure surface (kPa), c' is effective cohesion(kPa), ϕ' is effective internal friction angle (°), σ is total stress (kPa), u is pore water pressure (kPa).

The strength of the sliding soil is determined by the pore water pressure and the shear strength index c and φ during the process of rainfall infiltration. The expression for the shear strength of the soil is shown in Eq. (1). The variation curve of pore water pressure at the soil-bedrock interface of Qiling village landslide with time is shown in Fig. 31. Figure 31 shows that the pore water pressure gradually increased to its maximum during the two-day rainfall period, and, the pore water pressure gradually decreased again after the cessation of rainfall. To determine the variation law of the shear strength of the sliding zone soil with 2 days of rainfall and 2 days of no rainfall, saturation softening experiments were conducted on the sliding zone soil of the Qiling village landslide to obtain the soil moisture content at different saturation times, and the shear strength of the

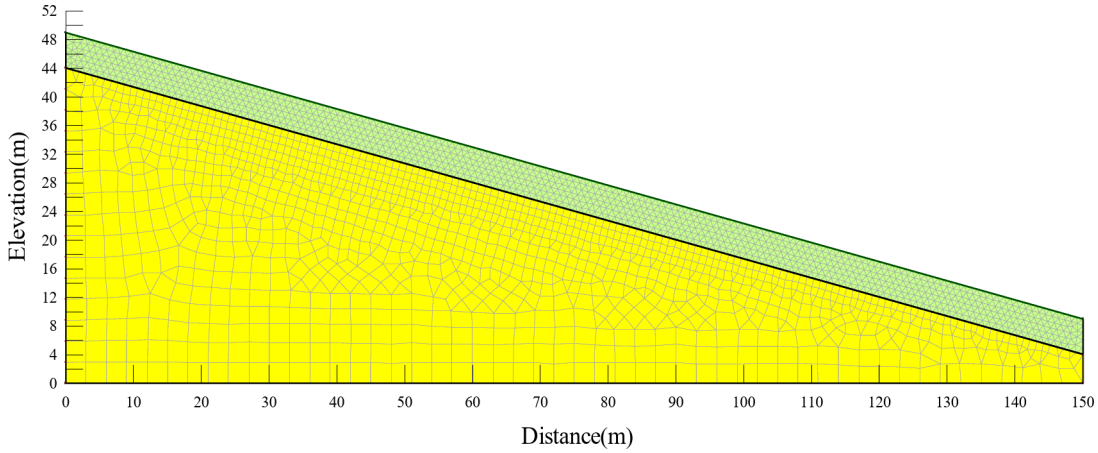

Fig. 24. Calculation model for a 5 m coverage layer.

Material	natural density/g/cm^3	cohesive force c (kPa)	internal friction angle φ/(°)	saturated volumetric water content(m^3/s^3)	residual volumetric water content(m^3/s^3)	Saturation permeability Coefficient (m/s)
Slippery soil	2.017	28	17	0.48	0.1	3.66×10^{-5}
Bedrock	SEEP/w	SLOP/w				6.94×10^{-9}
		nonskid surface				

Table 4. Parameters and relevant data adopted in the simulation.

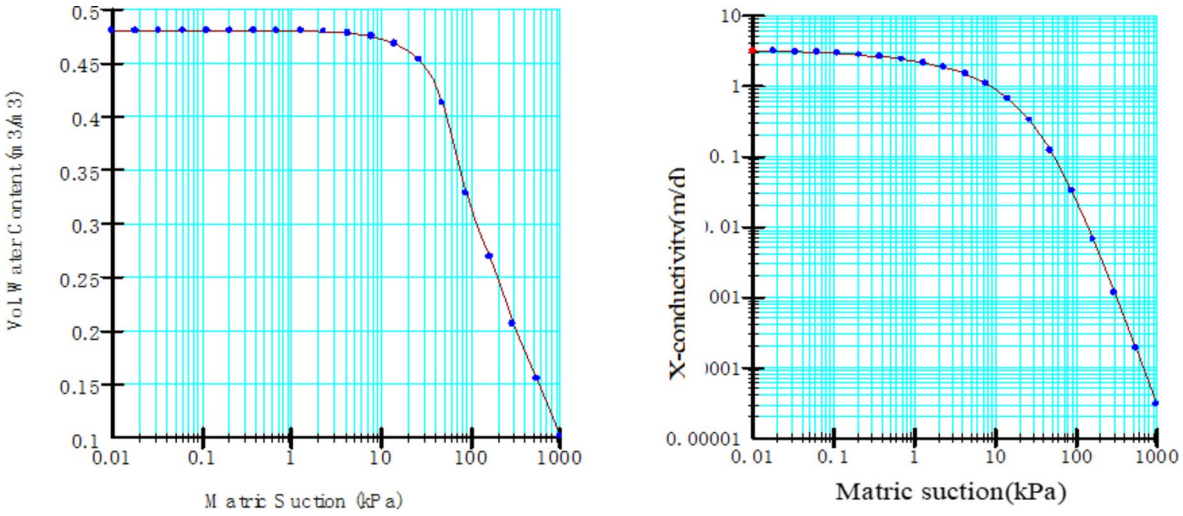

Fig. 25. Parameters in seepage analysis: (**a**) soil-water characteristic curve; (**b**) permeability curve.

soil at the corresponding moisture content was obtained through direct shear tests. The variation curve of soil shear strength with saturation time is shown in Fig. 32. Figure 32 show that the soil moisture content gradually increases and the soil shear streφngth gradually decreases with the soil saturation time increases within 0–48 h; the moisture content of the rain soil gradually decreases and the soil shear strength gradually increases after 48–96 h of air drying. The pore water pressure and shear strength index c and are substituted into Eq. (1) to calculate the strength of the soil at the soil-bedrock interface when it infiltrates with rainfall. The calculation result is shown in Fig. 33. Figure 33 show that the shear strength of the sliding soil gradually decreasesas rainfall continues within 0–48 h;, the shear strength of the sliding soil slowly increasesAfter the rainfall stops (48–96 h).

The limitations of two-dimensional numerical models in calculating landslide stability.Although the stability of the Qiling village landslide calculated by the two-dimensional numerical model is consistent with the results of field investigations. However, in areas with complex terrain structures and changes in property parameters, the calculation results of two-dimensional models often have certain deviations from the actual situation, while

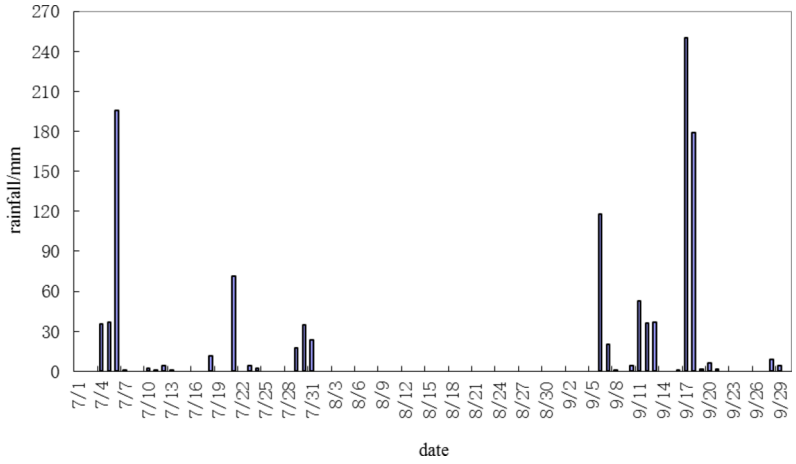

Fig. 26. Rainfall in Qiling village from July to September 2011.

the calculation results of three-dimensional models are consistent with the actual situation. Therefore, we will use a three-dimensional numerical model to analyze the seepage field and slope stability of the accumulation layer slope in future research in order to make the calculation results more consistent with the actual situation of landslides.

Conclusion

This study investigated the formation mechanisms of accumulative landslides sliding along the soil-bedrock interface in Nanjiang County via shear tests on sliding bodies, sliding zone soils, and bedrock interfaces with different moisture contents via a multifunctional testing instrument and an improved direct shear instrument. Using the Slope/w module and numerical simulation results of rainfall infiltration, the stability of the accumulative slope was analyzed, and the results are as follows:

(1) The shear strength of the interface between the sliding body, sliding zone soil, and bedrock decreased with increasing moisture content. The shear test results indicate that the shear strength at the interface between the sliding zone soil and the smooth bedrock is the smallest, revealing the reason why the Qiling Village landslide slid along the soil-bedrock interface.
(2) Under the action of heavy rainfall, rainwater flows from top to bottom. First, the soil saturates at the soil-bedrock interface at the front edge of the slope, forming a transient saturated seepage field. As the rainfall continues, the saturated area continuously moves from the front edge of the slope along the soil-bedrock interface toward the middle and rear parts of the slope, and the water level continues to rise, gradually increasing the pore water pressure.
(3) Under the action of heavy rainfall, owing to the existence of water infiltration channels in the soil, rainwater can quickly infiltrate the soil-bedrock interface, and the permeability of the bedrock is very low, playing a role in water isolation. Therefore, stagnant water is generated at the soil-bedrock interface, forming a transient water level. First, the front edge of the slope is saturated at the soil-bedrock interface, and as the rainfall continues, the saturated area continues to expand toward the middle and rear parts of the slope, and the water level line also continuously rises toward the surface.
(4) The coupling of pore water pressure and rainwater softening caused the Qiling Village landslide. The stability of the slope was greatly affected by pore pressure in the early stage of rainfall, and the influence of rainwater softening was greater in the later stage.

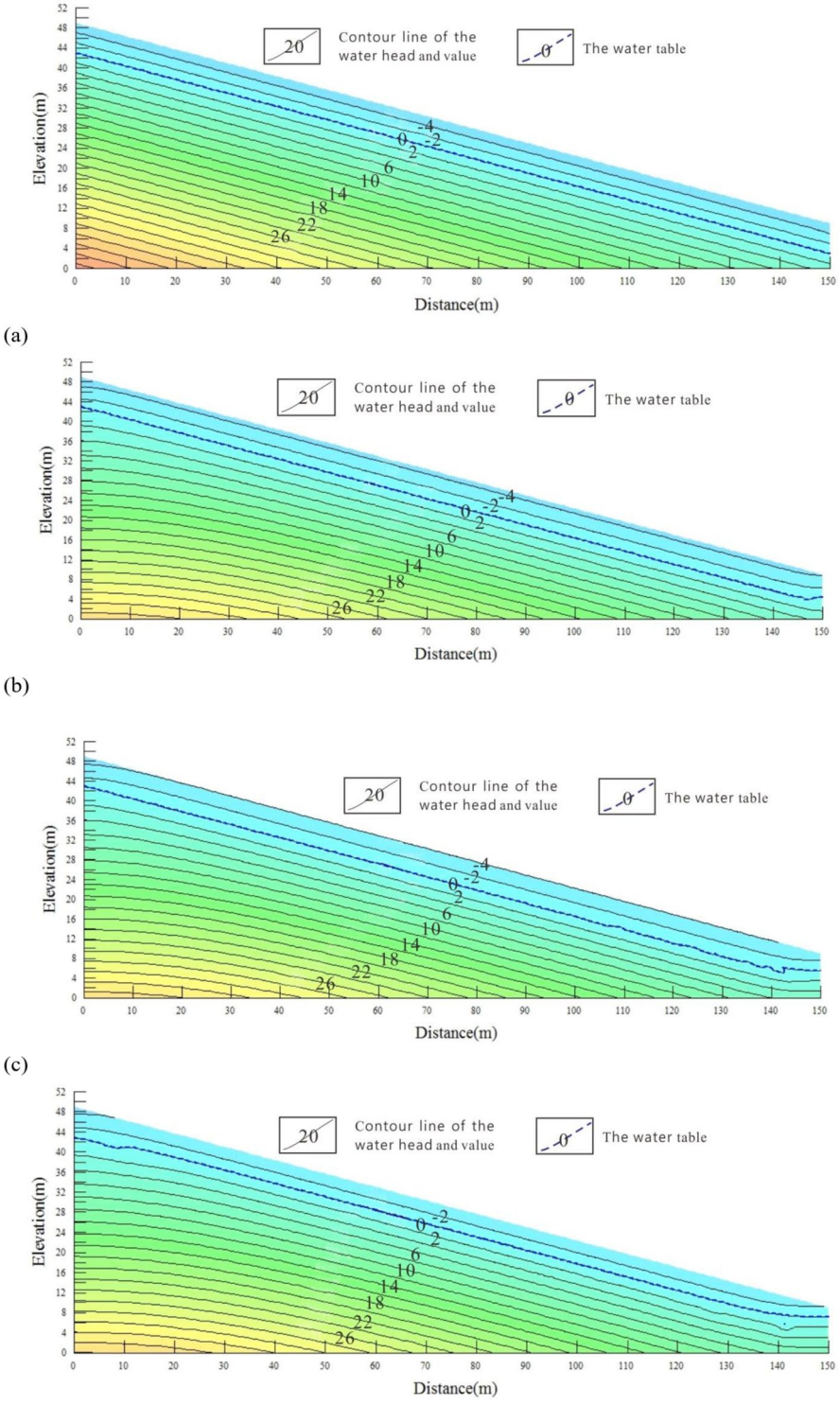

Fig. 27. Time variation of contour lines of the water head: (**a**) Initial state; (**b**) rainfall for 8 h; (**c**) 16 h of rainfall; (**d**) 24-hour rainfall; (**e**) 32 h of rainfall; (**f**) 40 h of rainfall; and (**g**) rainfall for 44 h.

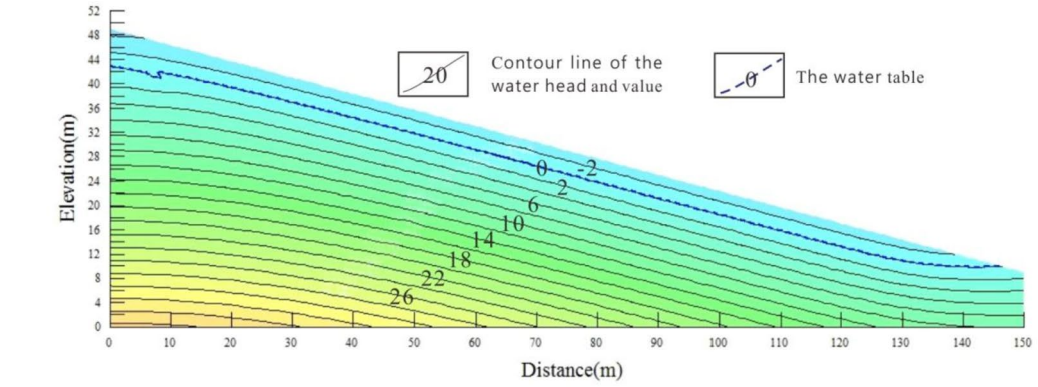

(e)

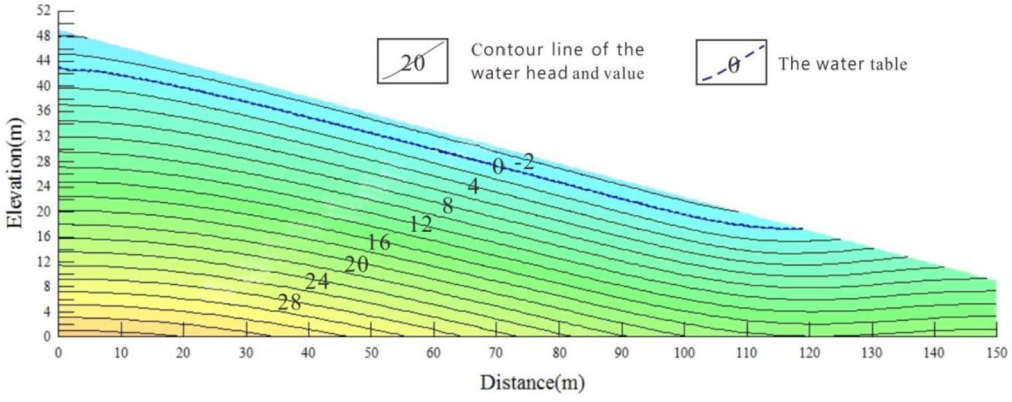

(f)

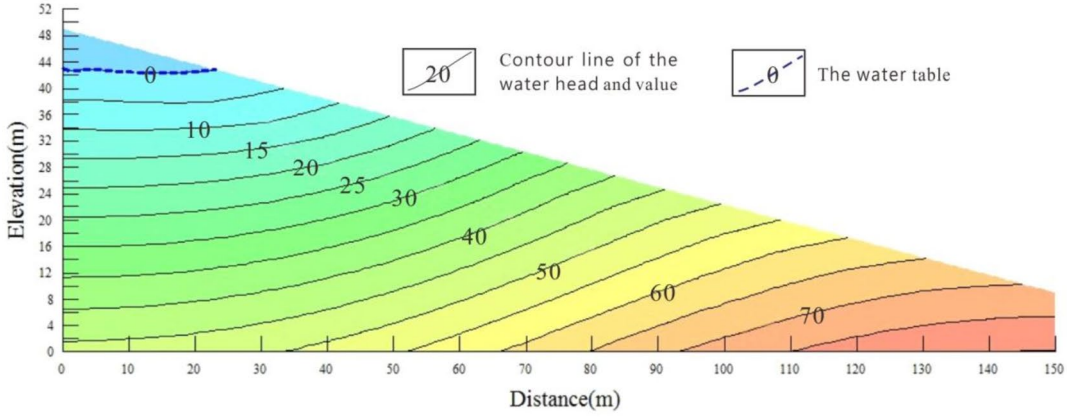

(g)

Figure 27. (continued)

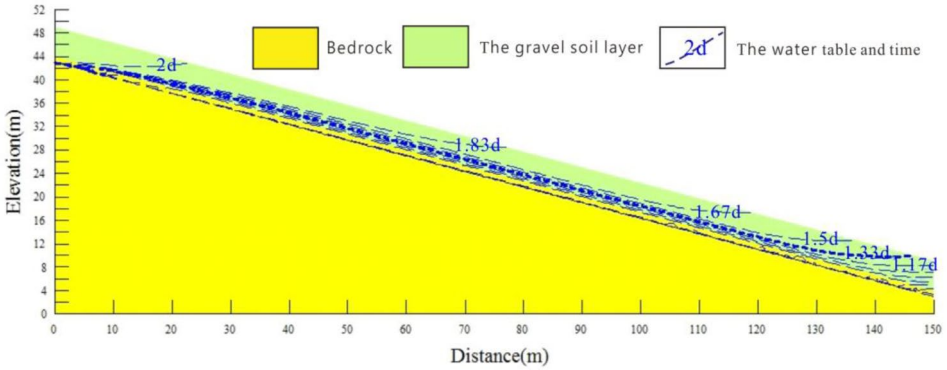

Fig. 28. Distribution of infiltration lines.

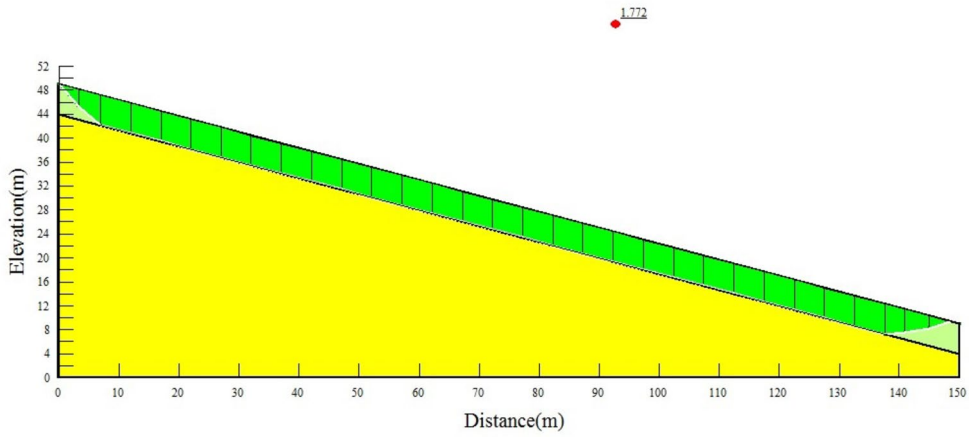

Fig. 29. Stability calculation of the 5-m overcover layer.

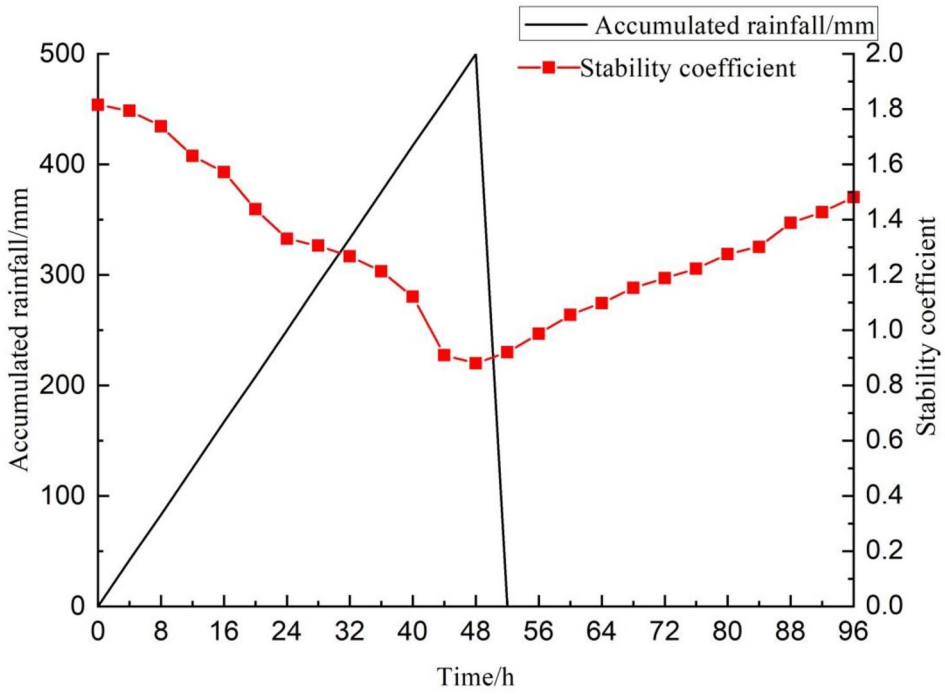

Fig. 30. Time-varying curve of the stability coefficient of the 5-m soil slope.

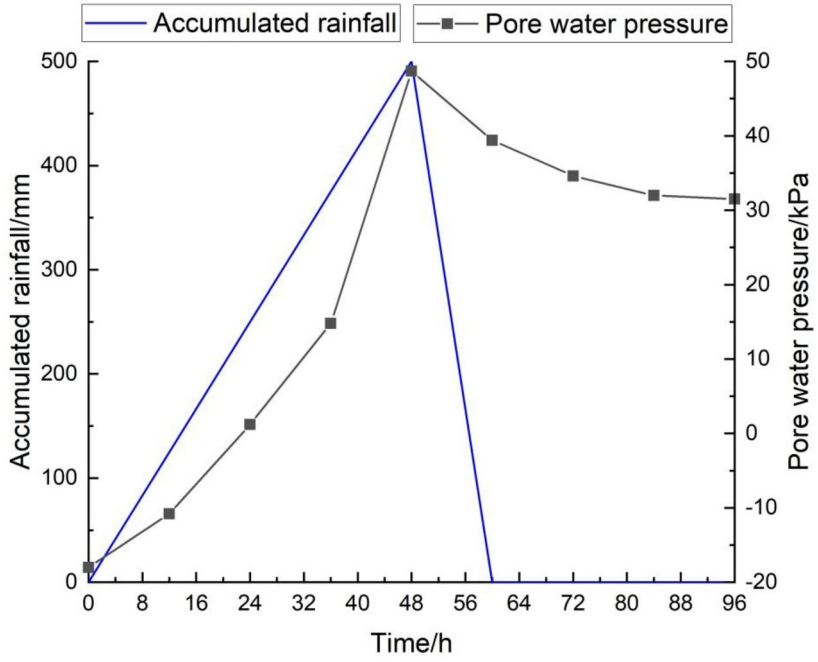

Fig. 31. Change in pore-water pressure with time.

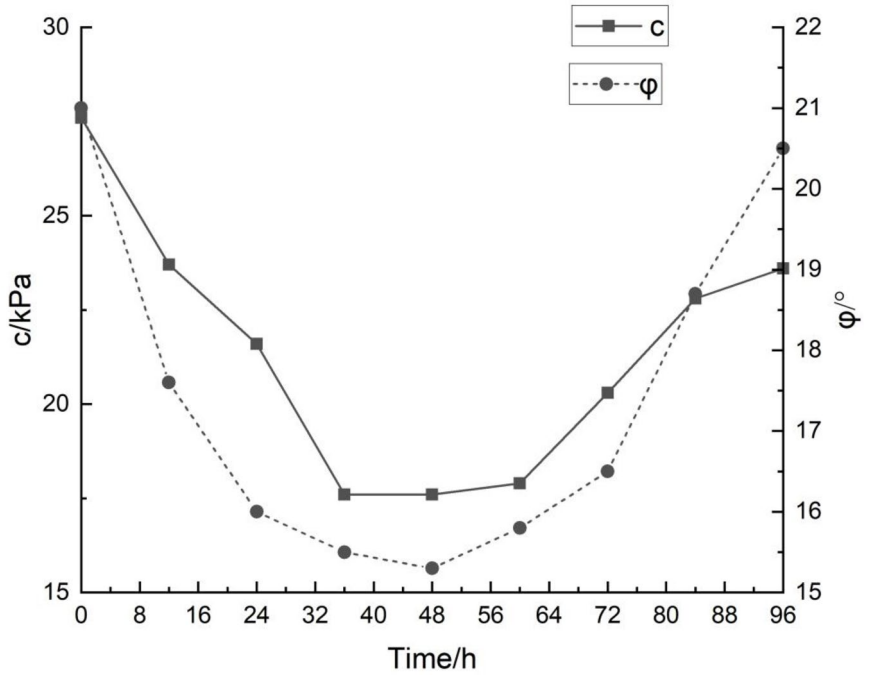

Fig. 32. The variation curve of shear strength value with saturation time.

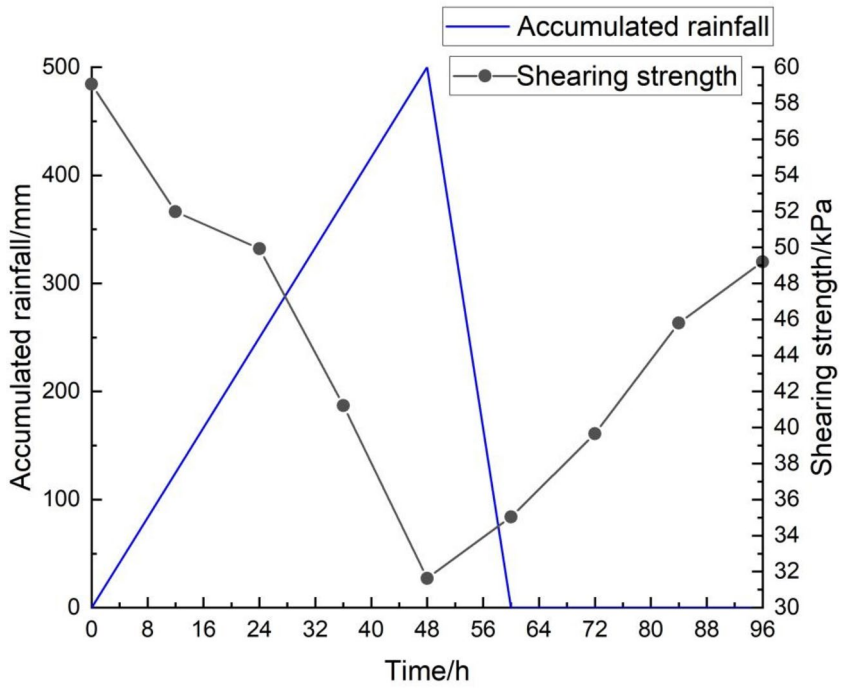

Fig. 33. The strength variation curve of sliding zone soil with rainwater infiltration time.

Data availability

The datasets used and/or analysed during the current study available from the corresponding author on reasonable request.

Received: 16 January 2025; Accepted: 9 April 2025
Published online: 30 April 2025

References

1. Zhou, W. Q. et al. Combining rainfall-induced shallow landslides and subsequent debris flows for hazard chain prediction. *Catena* **213**, 106199 (2022).
2. Sala, G., Lanfranconi, C., Frattini, P., Rusconi, G. & Crosta, G. B.Cost-sensitive rainfall thresholds for shallow landslides. *Landslides* **18** (9), 2979–2992 (2021).
3. Wu, Y. M., Lan, H. X., Gao, X., Li, L. P. & Yang, Z. H. A simplified physically based coupled rainfall threshold model for triggering landslides. *Eng. Geol.* **195**, 63–69 (2015).
4. Lan, H. X. et al. Climate change drives flooding risk increases in the yellow river basin. *Geogr. Sustain.* **5** (2), 193–199 (2024).
5. Balzano, B. et al. Building physically based models for assessing rainfall-induced shallow landslide hazard at catchment scale: case study of the Sorrento Peninsula (Italy). a*nadian geotechnical journal*.**56**(9):1291–1303 (2019).
6. Shen, D. Y., Shi, Z. M., Peng, M., Zhang, L. M. & Zhu, Y. Preliminary analysis of a rainfall-induced landslide hazard chain in Enshi City, Hubei Province, China in July 2020. *Landslides* **18** (1), 509–513 (2021).
7. Ling, C. P., Xu, Q., Zhang, Q., Ran, J. X. & Lv, H. B. Application of electrical resistivity tomography for investigating the internal structure of a translational landslide and characterizing its groundwater circulation (Kualiangzi landslide, Southwest China. *J. Appl. GeophysicsJournal Appl. Geophys.* **131**, 154–162 (2016).
8. Ye, F. et al. The 8•21rainfall-induced Zhonghaicun landslide in Hanyuan County of China: surface features and genetic mechanisms. *Landslides* **18** (10), 3421–3443 (2021).
9. Zhou, C. et al. Catastrophic landslide triggered by extreme rainfall in Chongqing, China: July 13, 2020, Niuerwan landslide.*Landslides*.19(10):2397–2407 (2022).
10. Zhang, Q., Xu, Q. & Ning N.A study of the stability influence factors andcoupling for inclined-shallowsoil landslides under the condition of rainfall. *Hydrogeol. Eng. Geol.* **5**, 90–94 (2014). (in Chinese).
11. Zhang, Q. et al. Study on the rainfall threshold of red strata landslides in Bazhong,Sichuan using kriging interpolation method.the Chinese. *J. Geol. Hazard. Control.* **35** (4), 36–44 (2024). (in Chinese).
12. Xu, Q. et al. Hysteresis effect on the deep-seated landslide by rainfall: the case of the Kualiangzi landslide, China, In: G. Lollino (eds.). *Engineering Geology for Society and Territory*.2:1557–1562 (2015).
13. Xu, Q., Liu, H., Ran, J. & Li, W. Sun,X.Fieldmonitoringofgroundwater responses to heavy rainfalls and the early warning of the Kualiangzi landslide in Sichuan basin, Southwestern China. *Landslides* **13**, 1555–1570 (2016).
14. Zhang, M., Yin, Y. & Huang, B. Mechanism of rainfall-induced land slide in gently inclined red beds in the Eastern Sichuan basin, SW China. *Landslides* **12**, 973–983 (2015).
15. Zhang, M., Yin, Y. P. & Mauri, M. Dynamics of the 2008 earthquake triggered Wenjiagou creek rock avalanche, Qingping, Sichuan, China. *Eng. Geol.* **200**, 75–87 (2016).
16. Zhang, S., Xu, Q. & Hu, Z. M. Effects of rainwater softening on red mud stone of deep seated landslide, Southwest China. *Eng. Geol.* **204**, 1–14 (2016).
17. Zhang, S., Xu, Q. & Zhang Q.Failure characteristics of gently inclined shallow landslides in Nanjiang, Southwest of China. *Eng. Geol.* **217**, 1–1 (2017).
18. Wang, W. Z., Xu, Q., Zheng, G., Li, J. Y. & Luo, B. Y.Centrifugal model tests on sliding failure of gentle debris slope under rainfall. *Rock. Soil. Mech.* **1**, 87–95 (2016). (in Chinese).
19. Wang, W. Z., Xu, Q. & Zheng, H. J. Tests of saturated and unsaturated hydraulic parameters of accumulation soil in gently shallow land slide by the rainstorm: a case study of the Wangzhengbang land slide. *Geol. Sci. Technol. Inform.* **1**, 202–207 (2017). (in Chinese).
20. Xu, Q., Wang, W. Z., Li, L. T. & Cao, Y. D.Failure mechanism of gently inclined shallow landslides along the soil-bedrock interface on ring shear tests. *Bull. Eng. Geol. Environ.* **80**, 3733–3746 (2021).
21. Chen, J. Y., Zhang, J. S. & Li, J. Influence of interface roughness on mechanical properties of red clay-concrete interface. *J. Cent. South. Univ. (Science Technology)*. **47** (5), 1682–1688 (2016). (in Chinese).
22. Gianvito, S., Hu, W., Xu, Q. & Huang, R. Q. Shear-rate-dependent behavior of clayey bi-material interfaces at landslide stress levels. *Am. Geophys. Union*. **2**, 766–777 (2018).
23. Wang, H. L., Zhou, W. H., Yin, Z. Y. & Jie, X. X. Effect of grain size distribution of sandy soil on shearing behaviors at soil–structure interface. *J. Mater. Civ. Eng.* **31** (10), 04019238 (2019).
24. Zhou, W. J., Guo, Z., Wang, L. Z., Li, J. H. & Rui, S. J.Sand-steel interface behaviour under large-displacement and Cyclic shear. *Soil Dyn. Earthq. Eng.* **138**, 106352 (2020).
25. Gan, F., Bi, J., Cao, T., Liu, P. F. & Wang, C. L. Analysis of progressive failure between soil and structure interface in the direct shear test using a new method. *J. Test. Eval.* **49** (6), 3947–3969 (2021).
26. Liao, C. C., Liu, S. A. & Xia, X. H.Triaxial shear test for strength behavior of saturated sand-steel interface based on preformed failure plane. *Geotech. Test. J.* **45** (5), 1005–1029 (2022).
27. Tsubakihara, Y. & Kishida, H. Frictional behaviour between normally consolidated clay and steel by two direct shear type apparatuses. *Soils Found.* **2**, 1–13 (1993).
28. Zhang, G. & Zhang, J. M. Monotonic and Cyclic tests of interface between structure and gravelly soil. *Soils Found.* **4**, 505–518 (2006).
29. Bacas, B. M. & Konietzky, C. J. Shear strength behavior of geotextile/geomembrane interfaces. *J. Rock. Mech. Geotech. Eng.* **6**, 638–645 (2015).
30. Yao, B., Li, F. C., Wang, X. & Chen G.Evaluation of the shear characteristics of steel–asphalt interface by a direct shear test method. *Int. J. Adhes. Adhes.* **68**, 70–79 (2016).
31. Liu, Y. et al. Experimental evaluation of the shear performance of steel-asphalt interface considering temperature and humidity coupling. *Int. J. Adhes. Adhes.* **84**, 360–367 (2018).
32. Bao, H. et al. Spatio-temporal evolution law of anisotropic shear damage on rock mass joint surface affected by joint morphology. *Eng. Fail. Anal.* **165**, 108820 (2024).
33. Han, C., Liu, X. L., Li, D. J. & Wang, J. W. J.Investigation on failure characteristic and instability mechanism of red sandstone including serrated joints under variable angle shear. *Arab. J. Geosci.* **15**, 124 (2022).
34. Bao, H. et al. Discrete element modeling method for anisotropic mechanical behavior of biotite quartz schist based on mineral identification technology. *Bull. Eng. Geol. Environ.* **84**, 28 (2025).
35. Tan, Z. Y. et al. Stability assessment of shallow soil landslide and activating rainfall threshold. *Nat. Hazards Rev.* **25** (2), 04024004 (2024).
36. Song, Y. S. H.S.Experimental study to estimate the criteria for shallow landslides under various geological conditions in South Korea. *Environ. Earth Sci.* **82**, 582 (2023).
37. Xiang, X. et al. Analyzing failure mechanisms and predicting step-like displacement: rainfall and RWL dynamics in lock-unlock landslides. *Geosci. Front.* **16**, 101959 (2025).
38. Tan, Y. L. et al. Slope stability analysis of saturated-unsaturated based on the GEO-studio: a case study of Xinchang slope in Lanping County, Yunnan Province. *China Environ. Earth Sci.* **82** (13), 322–322 (2023).

Acknowledgements

This work was supported by Hebei Natural Science Foundation [grant number D2023403055], Funding for the

Science and Technology Innovation Team Project of Hebei GEO University[grant number KJCXTD-2021-08].

Author contributions

X.L., wrote the content of this paper. corresponding author W.W., put forward the main research ideas of this paper, and wrote the main content of this paper. Y. H., M.Z., and R. Z., refined the research content of this paper and drew the corresponding chart files. Z.T., was mainly responsible for the typesetting of this article. M.H., was mainly responsible for guiding theoretical knowl-edge. J. Z., was mainly responsible for checking the typesetting and logic of this article.

Declarations

Competing interests

The authors declare no competing interests.

Additional information

Correspondence and requests for materials should be addressed to W.W.

Reprints and permissions information is available at www.nature.com/reprints.

Publisher's note Springer Nature remains neutral with regard to jurisdictional claims in published maps and institutional affiliations.